Porous silicon ring resonator for compact, high sensitivity biosensing applications

Gilberto A. Rodriguez,[1,*] Shuren Hu,[2] and Sharon M. Weiss,[1,2]

[1]*Department of Electrical Engineering and Computer Science, Vanderbilt University, Nashville, Tennessee 37235, USA*

[2]*Department of Physics and Astronomy, Vanderbilt University, Nashville, Tennessee 37240, USA*

[*]*gilberto.a.rodriguez@vanderbilt.edu*

Abstract: A ring resonator is patterned on a porous silicon slab waveguide to produce a compact, high quality factor biosensor with a large internal surface area available for enhanced recognition of biological and chemical molecules. The porous nature of the ring resonator allows molecules to directly interact with the guided mode. Quality factors near 10,000 were measured for porous silicon ring resonators with a radius of 25 μm. A bulk detection sensitivity of 380 nm/RIU was measured upon exposure to salt water solutions. Specific detection of nucleic acid molecules was demonstrated with a surface detection sensitivity of 4 pm/nM.

OCIS codes: (130.6010) Sensors; (130.3120) Integrated optics devices.

References and links

1. C. F. Carlborg, K. B. Gylfason, A. Kaźmierczak, F. Dortu, M. J. Bañuls Polo, A. Maquieira Catala, G. M. Kresbach, H. Sohlström, T. Moh, L. Vivien, J. Popplewell, G. Ronan, C. A. Barrios, G. Stemme, and W. van der Wijngaart, "A packaged optical slot-waveguide ring resonator sensor array for multiplex label-free assays in labs-on-chips," Lab Chip **10**(3), 281–290 (2010).
2. M. Iqbal, M. A. Gleeson, B. Spaugh, F. Tybor, W. G. Gunn, M. Hochberg, T. Baehr-Jones, R. C. Bailey, and L. C. Gunn, "Label-free biosensor arrays based on silicon ring resonators and high-speed optical scanning instrumentation," IEEE J. Sel. Top. Quantum Electron. **16**(3), 654–661 (2010).
3. W. Bogaerts, P. DeHeyn, T. Van Vaerenbergh, K. De Vos, S. K. Selvaraja, T. Claes, P. Dumon, P. Bienstman, D. Van Thourhout, and R. Baets, "Silicon microring resonators," Laser Photon. Rev. **6**(1), 47–73 (2012).
4. F. Dell'Olio and V. M. N. Passaro, "Optical sensing by optimized silicon slot waveguides," Opt. Express **15**(8), 4977–4993 (2007).
5. T. Claes, J. G. Molera, K. De Vos, E. Schacht, R. Baets, and P. Bienstman, "Label-free biosensing with a slot-waveguide-based ring resonator in silicon on insulator," IEEE Photon. J. **1**(3), 197–204 (2009).
6. M. Mancuso, J. M. Goddard, and D. Erickson, "Nanoporous polymer ring resonators for biosensing," Opt. Express **20**(1), 245–255 (2012).
7. C. Wongmanerod, S. Zangooie, and H. Arwin, "Determination of pore size distribution and surface area of thin porous silicon layers by spectroscopic ellipsometry," Appl. Surf. Sci. **172**(1-2), 117–125 (2001).
8. C. Pacholski, M. Sartor, M. J. Sailor, F. Cunin, and G. M. Miskelly, "Biosensing using porous silicon double-layer interferometers: reflective interferometric fourier transform spectroscopy," J. Am. Chem. Soc. **127**(33), 11636–11645 (2005).
9. K.-P. S. Dancil, D. P. Greiner, and M. J. Sailor, "A porous silicon optical biosensor: detection of reversible binding of IgG to a protein A-modified surface," J. Am. Chem. Soc. **121**(34), 7925–7930 (1999).
10. K. Kim and T. E. Murphy, "Porous silicon integrated Mach-Zehnder interferometer waveguide for biological and chemical sensing," Opt. Express **21**(17), 19488–19497 (2013).
11. X. Wei and S. M. Weiss, "Guided mode biosensor based on grating coupled porous silicon waveguide," Opt. Express **19**(12), 11330–11339 (2011).
12. P. A. Snow, E. K. Squire, P. St. J. Russel, and L. T. Canham, "Vapor sensing using the optical properties of porous silicon Bragg mirrors," J. Appl. Phys. **86**(4), 1781–1784 (1999).
13. S. Chan, P. M. Fauchet, Y. Li, L. J. Rothberg, and B. L. Miller, "Porous silicon microcavities for biosensing applications," Phys. Status Solidi, A Appl. Res. **182**(1), 541–546 (2000).
14. S. Li, D. Hu, J. Huang, and L. Cai, "Optical sensing nanostructures for porous silicon rugate filters," Nanoscale Res. Lett. **7**(79), 79 (2012).
15. G. A. Rodriguez, J. D. Ryckman, Y. Jiao, and S. M. Weiss, "A size selective porous silicon grating-coupled Bloch surface and sub-surface wave biosensor," Biosens. Bioelectron. **53**, 486–493 (2014).

#231054 - $15.00 USD Received 19 Dec 2014; revised 24 Feb 2015; accepted 28 Feb 2015; published 9 Mar 2015

16. S. Hu, Y. Zhao, K. Qin, S. T. Retterer, I. I. Kravchenko, and S. M. Weiss, "Enhancing the sensitivity of label-free silicon photonic biosensors through increased probe molecule density," ACS Photon. **1**(7), 590–597 (2014).
17. X. Wei and S. M. Weiss, "Grating coupled waveguide biosensor based on porous silicon," Proc. MRS **1301**, 219–224 (2011).
18. Y. A. Vlasov and S. J. McNab, "Losses in single-mode silicon-on-insulator strip waveguides and bends," Opt. Express **12**(8), 1622–1631 (2004).
19. X. Wei, J. W. Mares, Y. Gao, D. Li, and S. M. Weiss, "Biomolecule kinetics measurements in flow cell integrated porous silicon waveguides," Biomed. Opt. Express **3**(9), 1993–2003 (2012).
20. J. W. Mares and S. M. Weiss, "Diffusion dynamics of small molecules from mesoporous silicon films by real-time optical interferometry," Appl. Opt. **50**(27), 5329–5337 (2011).
21. A. J. Qavi, T. M. Mysz, and R. C. Bailey, "Isothermal discrimination of single-nucleotide polymorphisms via real-time kinetic desorption and label-free detection of DNA using silicon photonic microring resonator arrays," Anal. Chem. **83**(17), 6827–6833 (2011).
22. J. L. Lawrie, Z. Xu, G. Rong, P. E. Laibinis, and S. M. Weiss, "Synthesis of DNA oligonucleotides in mesoporous silicon," Phys. Status Solidi., A Appl. Mater. Sci. **206**(6), 1339–1342 (2009).
23. K. R. Beavers, J. W. Mares, C. M. Swartz, Y. Zhao, S. M. Weiss, and C. L. Duvall, "In situ synthesis of peptide nucleic acids in porous silicon for drug delivery and biosensing," Bioconjug. Chem. **25**(7), 1192–1197 (2014).
24. Y. Zhao, J. L. Lawrie, K. R. Beavers, P. E. Laibinis, and S. M. Weiss, "Effect of DNA-induced corrosion on passivated porous silicon biosensors," ACS Appl. Mater. Interfaces **6**(16), 13510–13519 (2014).
25. S. M. Grist, S. A. Schmidt, J. Flueckiger, V. Donzella, W. Shi, S. Talebi Fard, J. T. Kirk, D. M. Ratner, K. C. Cheung, and L. Chrostowski, "Silicon photonic micro-disk resonators for label-free biosensing," Opt. Express **21**(7), 7994–8006 (2013).

1. Introduction

Optical biosensors based on microring resonators are among the most promising biosensor platforms due to their long temporal light-matter interaction with surface bound molecules leading to competitive refractometric detection sensitivities, their ability to be cascaded together to make arrays, and their compact size for integration into portable lab-on-a-chip platforms. In particular, silicon-on-insulator (SOI) rings have been well-characterized and demonstrated for the detection and kinetics analysis of various chemical and biological molecules relevant to the military, the environment, food safety, and medical applications [1, 2]. The primary limiting factor for the detection sensitivity of traditional ring resonator sensors (typically near 160 nm/RIU or 0.158 nm/nm [2, 3]) is related to their fabrication on planar SOI and polymer materials. For planar materials, the majority of the electric field distribution associated with a waveguide (WG) mode is inside the WG, which is inaccessible to chemical and biological molecules; spatial overlap of target molecules and the optical mode occurs only at the WG surface where the evanescent tail of the mode exists [4]. Approaches to overcome this challenge have been pursued, including incorporating a slot in the WG ring or exciting the transverse magnetic (TM) mode to create a discontinuous electric field at interface between the guiding layer and surface, which generates a stronger molecular interaction with the evanescent tail of the mode. These design approaches have led to improved detection sensitivities near 246 nm/RIU and 0.290 nm/nm, respectively, for ring resonator sensors [1, 3, 5]. In this work, an alternate strategy of using a porous material, porous silicon (PSi), for the ring resonator waveguide is pursued to allow molecular infiltration into the guiding layer for direct interaction of target molecules with the resonant optical mode.

The only prior report of using a porous material for ring resonator structures is for a porous polymer ring resonator; however, the TM measurements performed and the very low porosity achievable for the polymer resulted in only a 94 nm/RIU bulk sensitivity [6]. PSi is the chosen material in this work due to its large internal surface area, tunable optical properties including a large achievable refractive index contrast between adjacent layers, low cost compared to SOI, and extensive surface functionalization chemistry available for the capture of relevant target molecules. PSi films have been demonstrated to have surface areas exceeding 180 m^2/cm^3, leading to improved molecular capture over planar transducer materials [7]. The porosity (refractive index), layer thickness, and number of layers can be controlled by electrochemical etching of p- or n- type silicon. This simple, cost-effective

#231054 - $15.00 USD Received 19 Dec 2014; revised 24 Feb 2015; accepted 28 Feb 2015; published 9 Mar 2015

fabrication process has led to the fabrication of several optical structures for sensing and other applications, including single and double layer interferometers [8, 9], Mach Zehnder interferometers [10], WGs [11], Bragg mirrors [12], microcavities [13], rugate filters [14], and Bloch surface wave structures [15].

In this work, we demonstrate, for the first time, the PSi ring resonator structure and its application for chemical and biomolecular sensing. The PSi ring resonator exhibits more than a factor of two greater bulk detection sensitivity and a one order of magnitude improvement in surface sensitivity for specific molecular detection compared to traditional SOI ring resonators. In section 2, we present the design, fabrication, measurement setup, surface functionalization method, and analyte preparation procedures. In section 3, we report on the characterization of the PSi ring resonator through computations and experiments, and we demonstrate its capabilities as a highly sensitive biosensor.

2. Methods

2.1 Design

Figure 1 shows a schematic of the ring resonator and identifies the various design parameters. Rings with radius size r = 10 μm and 25 μm are patterned with coupling gaps, g = 200 nm. The 200 nm gap size was experimentally tuned to achieve critical coupling. The effective index method was used to design a WG with a single TE mode. The ring WG width, w_{wg}, is 1.2 μm with height, h_{wg} = 600 nm and $h_{cladding}$ = 1.4 μm on a silicon substrate as shown in the inset of Fig. 1. The design consists of a double layer PSi WG on a silicon substrate with refractive indices n_{wg} = 1.79, $n_{cladding}$ = 1.24, and n_{sub} = 3.5, respectively. In addition, the ridge WG is tapered linearly from w_{taper} = 20 μm to w_{wg} = 1.2 μm over a length l_{taper} = 500 μm to reduce coupling losses. The 1.2 μm WG width is extended for l_{wg} = 1.2 mm with the ring of corresponding radius located at the center.

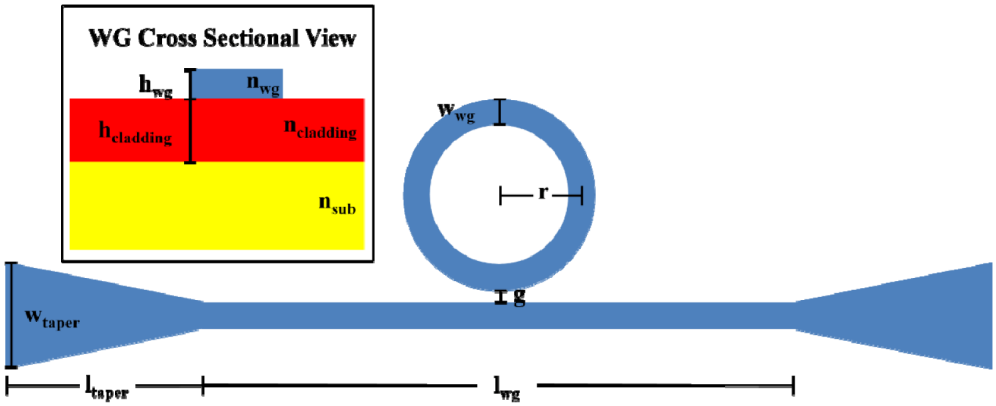

Fig. 1. Labeled schematic of PSi ring resonator employed in this work.

2.2 PSi ring resonator fabrication

PSi slab WGs were fabricated by electrochemical etching of p + (0.01 Ω·cm) Si (100) wafers in a 15% solution of hydrofluoric acid (HF) in ethanol. The guiding layer was created by applying a 5 mA/cm^2 current density for 114 seconds. The cladding layer was then etched at 48 mA/cm^2 for 53 seconds. A 1.5 mM·L^{-1} potassium hydroxide solution in ethanol was placed on each PSi WG for five minutes to widen the pores to improve molecular infiltration. Finally, the samples were oxidized at 500°C in air for five minutes to activate the surface for subsequent chemical functionalization. The resulting WGs had a 600 nm thick guiding layer with refractive index of 1.79 and a 1450 nm thick cladding layer with refractive index of 1.24.

#231054 - $15.00 USD Received 19 Dec 2014; revised 24 Feb 2015; accepted 28 Feb 2015; published 9 Mar 2015

The thicknesses were determined from SEM images and the refractive index parameters were determined by fitting reflectance spectra with transfer matrix simulations.

Rings were patterned on the slab waveguides using standard electron beam lithography (EBL) and reactive ion etching (RIE). EBL resist, ZEP 520A, was spun at 5000 rpm onto each PSi sample to create a 300 nm resist film. The rings of various sizes were then patterned by a JEOL JBX-9300-100kV EBL tool, followed by a 30 second development in xylenes and IPA rinsing. The patterned rings were then etched with an Oxford Plasmalab 100 RIE tool using $C_4F_8/SF_6/Ar$ gases to transfer the ring pattern into the guiding layer of the PSi WG. It was found that the short thermal oxidation step facilitated etching smooth sidewalls of the PSi ring resonator. Finally, a 10 minute O_2 plasma clean was performed to remove residual ZEP 520A resist. A scanning electron microscope (SEM) image of the entire ring (Fig. 2(a)), top view illustrating the different porosities of the guiding and cladding layers (Fig. 2(b)), and cross sectional view of the smooth PSi WG sidewall with photoresist on top of the high index layer (Fig. 2(c)) are shown. The rough interface between the high and low index layers in Fig. 2(c) is a result of the sample being manually cleaved.

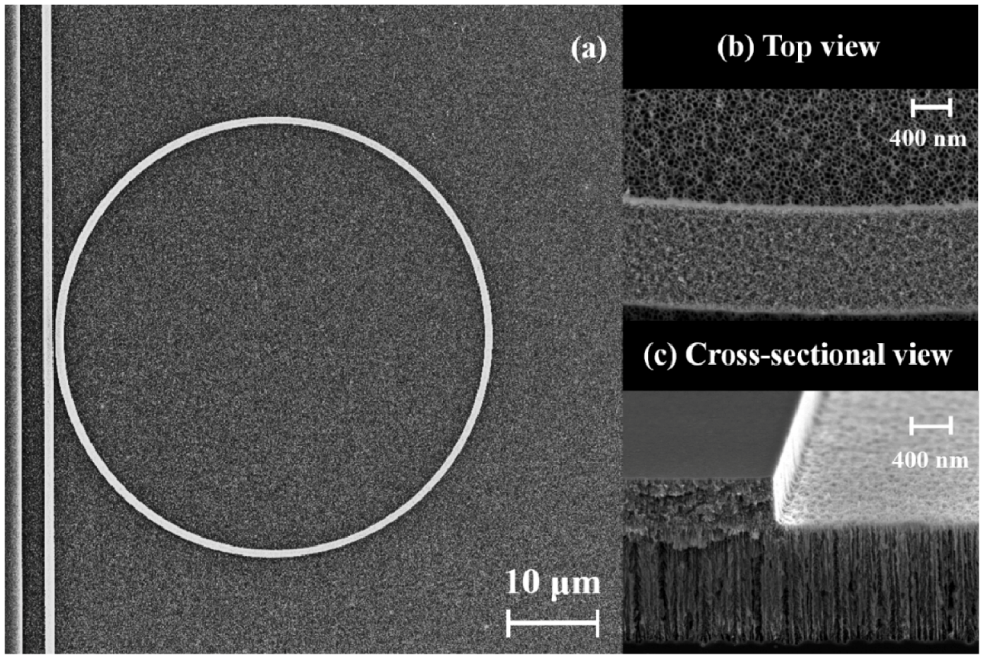

Fig. 2. SEM images of (a) 25µm radius PSi ring resonator WG, (b) top view porosity profile of the WG (small pores) and cladding (large pores) layers, and (c) cross section of the ridge WG post RIE etch.

2.3 Measurement setup

The PSi ring resonator chips were cleaved to an approximate 2.5 mm WG length and placed on a piezo-controlled XYZ stage. A tunable cw laser (Santec TSL-510) was coupled into the tapered ridge WG using lensed fiber (OZ Optics Ltd.). The TE polarized laser was swept from 1500 to 1630 nm with step size of 0.05 nm. The transmission was detected using a fiber-coupled photodiode receiver (Newport 2936-C). The tapered input and output fibers were positioned manually on each WG with the assistance of an infrared camera. All samples were measured at room temperature and a constant input power to minimize resonance wavelength fluctuations caused by thermo-optic effects. Additional reflectance measurements on unpatterned PSi slab WGs were performed on a Varian Cary 5000 UV-VIS-NIR spectrophotometer. The unpatterned PSi slab WG was exposed to the same processing

#231054 - $15.00 USD Received 19 Dec 2014; revised 24 Feb 2015; accepted 28 Feb 2015; published 9 Mar 2015

conditions as the PSi ring resonator described in section 2.2, with the exception of the EBL exposure step such that no pattern was transferred to the slab waveguide.

2.4 Surface functionalization

The bulk sensitivity of the PSi ring resonators was determined by exposure to several salt water concentrations. Refractive indices of the salt water solutions were found using a birefringence refractometer (Leice Abbe II). A 7.5 μL aliquot of each salt water solution was drop cast on the PSi ring resonators to ensure complete coverage of the rings during measurements. The PSi rings remained wet throughout the transmission measurements. In order to verify that the salt water concentration stayed constant during the measurements, control experiments were performed in which the time-dependent shift of the resonance wavelength was measured after a salt water solution was drop-cast onto the PSi ring resonator. Less than a 0.01 nm shift was observed during the first minute, corresponding to the measurement window for the bulk sensitivity measurements, confirming that evaporation effects are negligible. Following each salt water solution measurement, the PSi rings were rinsed with deionized (DI) water to remove residual salt from within the porous matrix, and then dried with nitrogen gas.

The surface sensitivity of the PSi rings was determined through specific detection of 16mer target peptide nucleic acid (PNA). Similar to Ref [16], a 4% solution of 3-aminopropyltriethoxisilane (3-APTES) in methanol and water was placed on the rings for 15 minutes, and then the rings were rinsed with methanol, thermally annealed for 10 minutes at 100°C, and soaked in methanol for an additional 10 minutes. Next, a 4.0 mg/mL solution of succinimidyl 3-(2-pyridyldithio)propionate (SPDP) in ethanol is placed on the 3-APTES functionalized rings for 30 minutes, followed by a 30 minute soak in ethanol. SPDP is used as a linking molecule to immobilize 100 μM thiol-modified 16mer probe DNA (5′TAG CTA TGG TCC TCG T-3′) in 4-(2-hydroxyethyl)-1-piperazineethanesulfonic acid (HEPES) buffer. The DNA is reduced by immobilized tris(2-carboxyethyl)phosphine (TCEP) disulfide reducing gel (Pierce). The DNA solution is placed on the functionalized rings for 1 hour, followed by a 30 minute rinse in HEPES buffer. The prepared PSi ring resonator sensor is then submerged in a 500 nM solution of complementary PNA (ACG AGG ACC ATA GCT A) in DI water for one hour. Finally, the sample is soaked in DI water for 30 minutes to remove non-hybridized PNA strands and dried with nitrogen gas.

3. Results and discussion

3.1 Propagation and bending losses

The propagation losses were determined by measuring the maximum transmission of PSi ridge WGs of different lengths without coupling tapers or ring patterning. The fabrication procedure is identical to that specified for the PSi rings in Section 2.2 and the measurement procedure is identical to that specified in Section 2.3. The inset of Fig. 3 shows the propagation losses for two sets of identical PSi ridge WGs of lengths 2.53 mm, 3.38 mm, 4.33 mm, and 5.63 mm with the transmission referenced to the shortest WG. The variation in measured transmission for WGs of the same length is likely a result of the manual alignment of the fibers used for butt coupling with the 1.2 μm wide WG. The propagation loss for the 1.2 μm wide WG is estimated to be near 2.75 dB/mm at 1550 nm, as determined from the slope of the linear fit (R^2 = 0.87) shown in the inset of Fig. 3. This value agrees with previously reported propagation losses for PSi films with similar oxidation conditions [17]. Although it is possible to reduce the propagation losses to < 1.5 dB/mm by increasing the oxidation time, the Q-factor of the ring resonator would decrease due to the resulting reduced refractive index contrast between the two oxidized porous layers of the WG.

In order to estimate bending losses in the PSi ring resonators, PSi ridge WGs with two 90° bends were fabricated as shown in the SEM image in Fig. 3. The bending losses for 10 μm

#231054 - $15.00 USD Received 19 Dec 2014; revised 24 Feb 2015; accepted 28 Feb 2015; published 9 Mar 2015

and 25 μm radius bends were determined to be <1 dB/90° bend, as the propagation losses dominated in both cases, which is comparable to reports for SOI WGs [18].

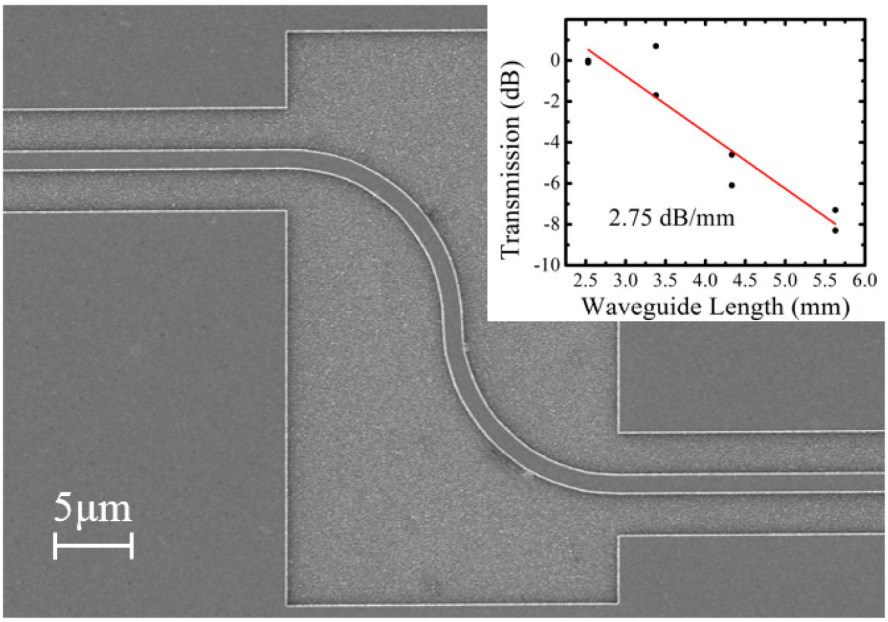

Fig. 3. SEM image of two 10 μm radius 90° bends in a PSi ridge WG used to characterize bending losses. Bending losses are estimated at <1 dB/90° bend. The inset image shows the relationship between measured transmission and PSi WG length, yielding PSi propagation losses of 2.75 dB/mm

3.2 Spectral characterization

Figure 4(a) presents the simulated and experimentally measured transmission spectra of a 25 μm radius PSi ring resonator. The simulated spectrum was obtained using 3-dimensional finite-difference time-domain (FDTD) analysis with the WG parameters given in section 2.1. The experimentally measured spectrum is in good agreement with simulation and shows a 7.6 nm free spectral range (FSR). The small, 40 pm deviation in resonance position is attributed to a slight difference in the simulated and actual PSi refractive index profile. A 2 nm deviation in resonance position was observed amongst all measured samples, which is attributed to slight variations in fabrication conditions. The Q-factor of the 25 μm radius PSi ring is estimated to be 9100 based on a Lorentzian fit of the measured resonance shown in Fig. 4(b). The Q-factor for the 10 μm radius PSi ring is 6400 near 1557 nm with a FSR of 18.8 nm, as shown in Fig. 4(c). In an aqueous environment, the Q-factors of the 10 μm and 25 μm PSi rings were estimated to be 3400 and 4000, respectively. The lower Q-factors in water are a result of water infiltrating the pores, which reduces the refractive index contrast between the two layers of the PSi WG.

#231054 - $15.00 USD Received 19 Dec 2014; revised 24 Feb 2015; accepted 28 Feb 2015; published 9 Mar 2015

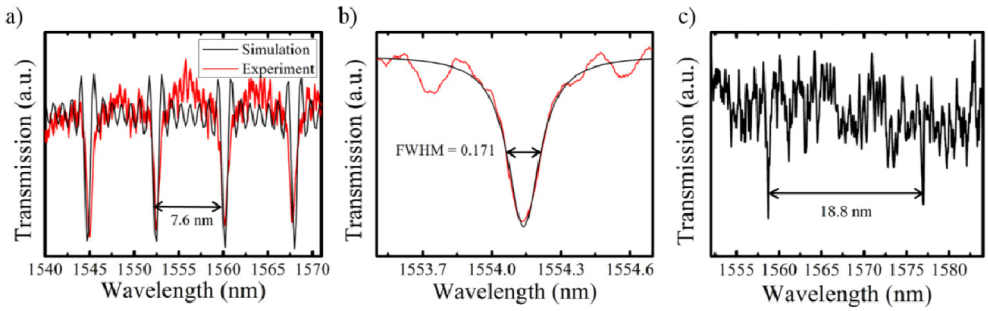

Fig. 4. (a) FDTD simulation (black) compared to measured transmission spectrum (red) of a 25 μm PSi ring. Good agreement of FSR = 7.6 nm and resonance wavelengths is observed. (b) Lorenzian fit of resonance near 1554 nm, which indicates a Q-factor of 9100. (c) Transmission spectrum of a 10 μm PSi ring with FSR = 18.8 nm and Q-factor of 6400 near 1558 nm.

3.3 Bulk sensitivity measurements

Exposure to different salt water solutions is a common approach for determining the bulk sensitivity of a biosensor due to the well characterized refractive index of varying NaCl concentrations in water and the low cost of the mixtures [2, 19]. Accordingly, different salt water solutions are placed on PSi rings of 10 μm and 25 μm radius to determine their bulk sensitivity. The diffusion of the NaCl solution into the pores is nearly instantaneous due to the small size of NaCl [19, 20]. Transmission measurements are conducted immediately after the 7.5 μL aliquot is placed on each ring. Between each salt water measurement, the PSi ring is rinsed with DI water and the transmission spectrum is measured to verify that the resonances return to their initial wavelengths, confirming that no salt remains in the rings. The shift of each resonance upon exposure to a given salt water concentration is measured relative to the DI water reference resonance wavelength of the PSi ring. The bulk sensitivity of the PSi ring is then estimated by a linear fit to the data with R^2 values greater than 0.99. As shown in Fig. 5, the bulk sensitivity of the 10 μm radius PSi ring is 384 ± 3.7 nm/RIU and that of the 25 μm PSi ring is 380 ± 4.5 nm/RIU. The bulk sensitivity values are the largest reported for ring resonator sensors and are achieved because the porous nature of the ring allows the salt water to penetrate into the volume inside the ring where the majority of the optical mode is confined. The modal profile of a PSi WG and its sensitivity comparison to SOI WGs has been previously reported [11]. We believe this increased light-matter interaction in the pores is the dominant factor in the bulk sensitivity increase and that longer temporal interactions arising from the ring resonator geometry play only a minor role. Due to the large sensitivity of the PSi rings, the FSR becomes a limiting factor for the detection of very large index changes. Accordingly, the maximum detection limits of the 10 μm and 25 μm PSi rings are $\Delta n = 0.05$ and 0.02, respectively, for single point measurements such as those conducted in this work. Larger refractive index changes would result in a resonance shifting by more than one FSR, confounding quantitative analysis. This maximum limit of detection may be circumvented if a real-time measurement system using microfluidics to enable continuous monitoring is incorporated.

#231054 - $15.00 USD Received 19 Dec 2014; revised 24 Feb 2015; accepted 28 Feb 2015; published 9 Mar 2015

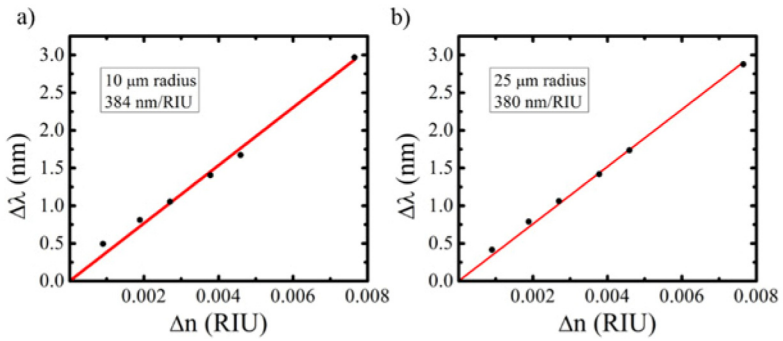

Fig. 5. Bulk sensitivity of (a) 10 μm and (b) 25 μm radius PSi ring resonators as determined based on exposure to different salt water concentrations referenced to deionized water. The sensitivity of both rings is approximately 380 nm/RIU

3.4 Surface sensing measurements

The APTES, SPDP, and probe DNA functionalization described in section 2.4 is performed to prepare the PSi ring resonators for detection of a 500 nM target PNA solution. Due to the large sensitivity (>1000 nm/RIU) of the PSi WG to small molecules in ambient conditions [11], the APTES and SPDP surface functionalization steps cannot be unambiguously quantified by the PSi rings resonators because the resonance shift exceeds the FSR; however, the detection of the aforementioned functionalization steps were verified by reflectance measurements on an unpatterned PSi slab WG. As shown in Fig. 6(a), the reflectance shift due to APTES and SPDP is 50 nm and 46 nm, respectively. APTES and SPDP are known to form monolayers of approximately 0.8 nm and 0.68 nm, respectively, which leads to the large spectral shift when they are attached to the internal pore walls. The 10 μm radius PSi ring (FSR ≈19 nm) can unambiguously detect the attachment of 100 μM probe DNA, which leads to a resonance shift of 11.10 nm, as shown in Fig. 6(b). This large concentration of probe DNA was used to ensure maximal probe coverage in the pores. Both the 10 μm and 25 μm radius PSi rings are able to detect the capture of 500 nM target PNA. As shown in Fig. 6(b) and Fig. 6(c), PNA hybridization leads to a resonance shift of 2.00 nm and 1.48 nm for the 10 μm and 25 μm radius PSi rings, respectively. The difference in resonance shift upon PNA attachment is attributed primarily to variation in molecular adsorption on the two samples. Based on the similar bulk sensitivity of the 10 μm and 25 μm radius PSi rings, it is anticipated that the surface sensitivity of the rings should be similar, as well. Accordingly, based on the experimental results, the surface sensitivity of the PSi ring resonators is approximately 4 pm/nM for detection of nucleic acid molecules. The high quality and high sensitivity of the rings demonstrates an order of magnitude increased detection sensitivity compared to traditional SOI ring resonator sensors [16, 21]. The detection sensitivity of PSi ring resonator sensors may be further improved by optimizing the probe molecule density in the pores using an in situ synthesis process for probe DNA or PNA attachment that yields increased DNA-PNA hybridization [22–24]. We calculate the limit of detection and intrinsic limit of detection for our device as reported in [1] and [25]. The limit of detection (3σ/sensitivity, where 3σ = 12 pm is the smallest spectral shift that can be reliably measured, as estimated by three times the standard deviation of the resonance wavelength drift due to temperature fluctuations and measurement system noise contributions) for target PNA is 3 nM. The intrinsic limit of detection (FWHM/sensitivity, where FWHM = 0.17 nm is the full-width at half-maximum of the PSi ring resonator resonance) is 42 nM.

#231054 - $15.00 USD Received 19 Dec 2014; revised 24 Feb 2015; accepted 28 Feb 2015; published 9 Mar 2015

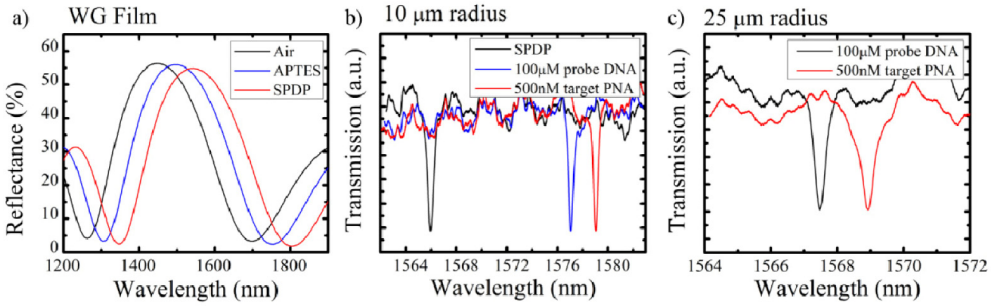

Fig. 6. (a) PSi slab WG reflectance fringe shifts caused by APTES and SPDP attachment. (b) Resonance shifts of 10 μm radius PSi ring due to attachment of DNA and PNA to a SPDP functionalized surface. (c) Transmission spectra of 25 μm radius PSi ring before and after DNA-PNA hybridization.

4. Conclusions

This work presents the first demonstration of a PSi ring resonator. Passive characterization of 10 μm and 25 μm PSi rings showed that the structures exhibit Q-factors near 10,000, propagation losses near 2.75 dB/mm, and bending losses less than 1 dB/90° bend. Active characterization of the PSi rings demonstrated a bulk detection sensitivity near 380 nm/RIU based on salt water measurements and a surface sensitivity near 4 pm/nM with a limit of detection of 3 nM based on nucleic acid detection. The superior sensing performance of PSi ring resonators compared to traditional ring resonators arises due to the enormous internal surface area of PSi and the resulting strong light-matter interaction between the guided mode and target molecules in the pores. The high detection sensitivity of relatively compact PSi ring resonators along with their capability to detect molecules in a liquid environment opens the door to future microfluidics integration and real-time lab-on-a-chip applications.

Acknowledgments

This work was funded in part by the Army Research Office (W911NF-09-1-0101) and National Science Foundation (ECCS-0746296). Lithography was conducted at the Center for Nanophase Materials Sciences, which is a DOE Office of Science User Facility. SEM was conducted at Vanderbilt Institute of Nanoscale Science and Engineering (NSF ARI-R2 DMR-0963361). The authors thank S. Retterer and D. Briggs for their fabrication expertise, and J. Pecyna and P. Kaszynski for their assistance using the birefringence refractometer.

#231054 - $15.00 USD Received 19 Dec 2014; revised 24 Feb 2015; accepted 28 Feb 2015; published 9 Mar 2015